Inorg. Chem. **2006**, *45*, 4626–4636

Ligand Effects on the Structures of Extended Networks of Dicyanamide-Containing Transition-Metal Ions

Donatella Armentano,[†] Giovanni De Munno,*[,†] Francesca Guerra,[†] Miguel Julve,*[,‡] and Francesc Lloret[‡]

Dipartimento di Chimica, Università della Calabria, via P. Bucci 14/c, 87036 Arcavacata di Rende, Cosenza, Italy and Departament de Química Inorgánica, Instituto de Ciencia Molecular, Facultat de Química de la Universitat de València, Dr. Moliner 50, 46100 Burjassot, València, Spain

Received January 9, 2006

The structural characterization of a series of complexes of formula $[M(dca)_2L]_n$, where dca = dicyanamide, L = 1,10-phenanthroline (phen) [**1**–**4**] and 2,9-dimethylphenanthroline (2,9-dmphen) [**9**–**12**], and M = Mn (**1** and **9**), Fe (**2** and **10**), Co (**3** and **11**), and Ni (**4** and **12**), has revealed the effect of the presence of the methyl substituents of L on the resulting network. The structure of $[Mn(dca)_2(phen)]_n$ (**1**), which is identical to those of **2**–**4**, together with the investigation of its magnetic properties in the temperature range of 77–300 K were reported elsewhere. The use of the 4,7-dimethylphenanthroline (4,7-dmphen) as the co-ligand yielded a series of compounds of formula $[M(dca)_2(4,7\text{-dmphen})]_n$ [M = Mn (**5**), Fe (**6**), Co (**7**), and Ni (**8**)], which are isostructural with **1**–**4**. Compounds containing phen (**1**–**4**) and 4,7-dmphen (**5**–**8**) are made of two-dimensional grids of metal atoms, each metal atom being linked to three other metal centers through single (three metal atoms involved) and double (two metal atoms involved) dca bridges exhibiting the μ-1,5 coordination mode. The isostructural complexes $[M(dca)_2(2,9\text{-dmphen})]_n$ (**9**–**12**) also have a sheetlike structure, the metal atoms in each layer being linked by two single and one double μ-1,5-dca units, as in **1**–**8**. However, the topology of the network in **9**–**12** is different from that in **1**–**8** because of the different arrangement of the two single μ-1,5 dca bridges: cis in **1**–**8** versus trans in **9**–**12**. The magnetic study of compounds **1**–**12** in the temperature range of 1.9–290 K has revealed the occurrence of weak ferromagnetic (M = Ni) and antiferromagnetic interactions (M = Mn, Fe, and Co). The different magnetic behavior in **1**–**12** was analyzed in the light of their structures, and the values of the magnetic interactions were compared to those of related systems.

Introduction

Crystal engineering of coordination polymers is a field of research that has recently gained considerable attention, in part, because of the promise of the rational design of molecule-based materials with novel magnetic or nonlinear optical properties.[1,2] One can systematically influence the topology of the resultant polymeric network by subtle changes of the ligand and the metal environment. Many new and exciting structures have been reported, often displaying unique architectures and intrincate entanglements.[3]

In recent years, much attention has been devoted to dicyanamide (dca)-bridged polynuclear systems because of the large variety of topologies and magnetic properties that result from the versatility of dca as a ligand (Scheme 1). The α-$M(dca)_2$ series of compounds, which has isomorphous rutile-like structure, displays ferromagnetism [Co (T_c = 9 K) and Ni (T_c = 20 K)],[4,5] spin-canted antiferromagnetism

* To whom correspondence should be addressed. E-mail: demunno@unical.it (G.D.M.); miguel.julve@uv.es (M.J.).
[†] Università della Calabria.
[‡] Universitat de València.

(1) (a) Brammer, L. *Chem. Soc. Rev.* **2004**, *33*, 476. (b) Braga, D. *Chem. Commun.* **2003**, 2751. (c) Batten, S. R. *Curr. Opin. Solid State Mater. Sci.* **2001**, *5*, 107.
(2) (a) Braga, D.; Grepioni, F.; Orpen, A. G. *Crystal Engineering: from Molecules and Crystals to Materials*; Kluwer Academic Publishers: Dordrecht, The Netherlands, 1999. (b) Braga, D.; Grepioni, F. *Coord. Chem. Rev.* **1999**, *183*, 19.
(3) (a) Blatov, V. A.; Carlucci, L.; Ciani, G.; Proserpio, D. M. *CrystEngComm* **2004**, *6*, 377. (b) Batten, S. R.; Robson, R. *Angew. Chem.—Int. Ed.* **1998**, *37*, 1461.

10.1021/ic060044u CCC: $33.50
Published on Web 05/17/2006

Scheme 1. Coordination Modes of the Dicyanamide Anion

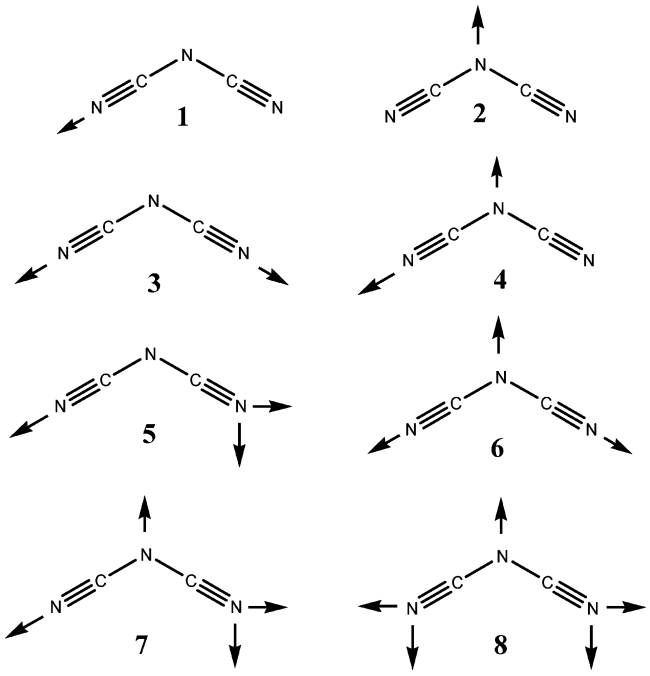

[Cr (T_N = 47 K), Mn (T_N = 16 K), and Fe (T_N =19 K)],[6] and paramagnetism (Cu).[5] The unusual magnetic properties of these compounds have encouraged the characterization of a large number of new coordination polymers containing the dca ligand and different auxiliary ligands which can be monodentate, polydentate or bridging.[7] Monodentate co-ligands (including coordinated solvent molecules) often give one-dimensional (1D) compounds with double dca bridges[8−13] and sometimes 2D arrays with single dca bridges.[11,13,14] Mononuclear species,[15,16] different types of chains,[8,11,17−21] and 2D motifs[16,22−26] have resulted in the presence of a chelating ligand. Compounds with a 3D structure have been observed more rarely.[22,27,28] The use of a bridging co-ligand increases the possibility to get two- or three-dimensional structures, as shown by the number of reports on 2D and intricate 3D networks which have been built in so doing.[23,29,30]

In most of the dca-containing metal complexes, this ligand features the end-to-end ($\mu_{1,5}$) bridging mode which has been proved to mediate weak magnetic interactions between the paramagnetic metal ions.[17] The key factors to enhance the magnetic coupling through this bridge are poorly understood and they remain a subject of intensive research.

(4) (a) Kmety, C. R.; Manson, J. L.; Huang, Q. Z.; Lynn, J. W.; Erwin, R. W.; Miller, J. S.; Epstein, A. J. *Mol. Cryst. Liquid Cryst*. **1999**, *334*, 631. (b) Manson, J. L.; Kmety, C. R.; Huang, Q. Z.; Lynn, J. W.; Bendele, G. M.; Pagola, S.; Stephens, P. W.; Liable-Sands, L. M.; Rheingold, A. L.; Epstein, A. J.; Miller, J. S. *Chem. Mater*. **1998**, *10*, 2552.

(5) (a) Batten, S. R.; Jensen, P.; Moubaraki, B.; Murray, K. S.; Robson, R. *Chem. Commun.* **1998**, 439. (b) Kurmoo, M.; Kepert, C. J. *New J. Chem.* **1998**, *22*, 1515.

(6) (a) Manson, J. L.; Kmety, C. R.; Palacio, F.; Epstein, A. J.; Miller, J. S. *Chem. Mater*. **2001**, *13*, 1068. (b) Kmety, C. R.; Huang, Q. Z.; Lynn, J. W.; Erwin, R. W.; Manson, J. L.; McCall, S.; Crow, J. E.; Stevenson, K. L.; Miller, J. S.; Epstein, A. J. *Phys. Rev. B* **2000**, *62*, 5576.

(7) (a) Batten, S. R.; Murray, K. S. *Coord. Chem. Rev.* **2003**, *246*, 103. (b) Miller, J. S.; Manson, J. L. *Acc. Chem. Res*. **2001**, *34*, 563. (c) Manson, J. L. Cooperative Magnetic Behavior in Metal-Dicyanamide Complexes. In *Magnetism: Molecules to Materials V*; Miller, J. S., Drillon, M., Eds.; Wiley-VCH Verlag GmbH & Co: Weinheim, Germany, 2005; p 71.

(8) (a) Ghoshal, D.; Ghosh, A. K.; Ribas, J.; Zangrando, E.; Mostafa, G.; Maji, T. K.; Chaudhuri, N. R. *Cryst. Growth Des*. **2005**, *5*, 941.

(9) (a) Luo, J.; Liu, B. S.; Zhou, X. G.; Weng, L. H.; Li, Y. R.; Cai, R. F. *Acta Crystallogr., Sect. E* **2004**, *60*, M1391. (b) Luo, J.; Liu, B. S.; Zhou, X. G.; Weng, L. H.; Li, Y. R.; Wua, H. X. *Acta Crystallogr., Sect. C* **2004**, *60*, M520. (c) Liu, C. M.; Zhang, D. Q.; Zhu, D. B.; Jin, X. L. *Transition Met. Chem.* **2003**, *28*, 336. (d) Sun, B. W.; Gao, S.; Ma, B. Q.; Wang, Z. M. *Inorg. Chem. Commun.* **2001**, *4*, 72. (e) Manson, J. L.; Arif, A. M.; Incarvito, C. D.; Liable-Sands, L. M.; Rheingold, A. L.; Miller, J. S. *J. Solid State Chem.* **1999**, *145*, 369. (f) Manson, J. L.; Arif, A. M.; Miller, J. S. *J. Mater. Chem.* **1999**, *9*, 979.

(10) Dong, W.; Liang, M.; Sun, Y. Q.; Liu, Z. Q. *Z. Anorg. Allg. Chem.* **2003**, *629*, 2443.

(11) Escuer, A.; Mautner, F. A.; Sanz, N.; Vicente, R. *Inorg. Chim. Acta* **2002**, *340*, 163.

(12) Escuer, A.; Mautner, F. A.; Sanz, N.; Vicente, R. *Inorg. Chem.* **2000**, *39*, 1668.

(13) Batten, S. R.; Jensen, P.; Kepert, C. J.; Kurmoo, M.; Moubaraki, B.; Murray, K. S.; Price, D. J. *J. Chem. Soc., Dalton Trans.* **1999**, 2987.

(14) (a) Dalai, S.; Mukherjee, P. S.; Zangrando, E.; Chaudhuri, N. R. *New J. Chem.* **2002**, *26*, 1185. (b) Manson, J. L.; Schlueter, J. A.; Geiser, U.; Stone, M. B.; Reich, D. H. *Polyhedron* **2001**, *20*, 1423.

(15) (a) Wu, A. Q.; Zheng, F. K.; Guo, G. C.; Huang, J. S. *Acta Crystallogr., Sect. E*. **2004**, *60*, M373. (b) Xu, J. Y.; Bian, H. D.; Wang, Q. L.; Gu, W.; Yan, S. P.; Liao, D. Z.; Cheng, P.; Jiang, Z. H.; Shen, P. W. *Z. Anorg. Allg. Chem.* **2003**, *629*, 1063. (c)He, Y.; Kou, H. Z.; Wang, R. J.; Li, Y. D.; Xiong, M. *Transition Met. Chem.* **2003**, *28*, 464. (d) Moliner, N.; Gaspar, A. B.; Munoz, M. C.; Niel, V.; Cano, J.; Real, J. A. *Inorg. Chem.* **2001**, *40*, 3986. (e) Wang, Z. M.; Luo, J.; Sun, B. W.; Yan, C. H.; Liao, C. S.; Gao, S. *Acta Crystallogr., Sect. C* **2000**, *56*, E242. (f) Potocnak, I.; Dunajjurco, M.; Miklos, D.; Kabesova, M.; Jager, L. *Acta Crystallogr., Sect. C* **1995**, *51*, 600.

(16) Mohamadou, A.; van Albada, G. A.; Kooijman, H.; Wieczorek, B.; Spek, A. L.; Reedijk, J. *New J. Chem.* **2003**, *27*, 983.

(17) Carranza, J.; Sletten, J.; Lloret, F.; Julve, M. *Inorg. Chim. Acta* **2004**, *357*, 3304.

(18) (a) Boca, R.; Boca, M.; Gembicky, M.; Jager, L.; Wagner, C.; Fuess, H. *Polyhedron* **2004**, *23*, 2337. (b) Paraschiv, C.; Sutter, J. P.; Schmidtmann, M.; Muller, A.; Andruh, M. *Polyhedron* **2003**, *22*, 1611. (c) Claramunt, A.; Escuer, A.; Mautner, F. A.; Sanz, N.; Vicente, R. *J. Chem. Soc., Dalton Trans.* **2000**, 2627.

(19) Vangdal, B.; Carranza, J.; Lloret, F.; Julve, M.; Sletten, J. *J. Chem. Soc., Dalton Trans.* **2002**, 566.

(20) Carranza, J.; Brennan, C.; Sletten, J.; Lloret, F.; Julve, M. *J. Chem. Soc., Dalton Trans.* **2002**, 3164.

(21) Marshall, S. R.; Incarvito, C. D.; Shum, W. W.; Rheingold, A. L.; Miller, J. S. *Chem. Commun.* **2002**, 3006.

(22) (a) Armentano, D.; De Munno, G.; Guerra, F.; Faus, J.; Lloret, F.; Julve, M. *Dalton Trans.* **2003**, 4626. (b) Konar, S.; Dalai, S.; Mukherjee, P. S.; Drew, M. G. B.; Ribas, J.; Chaudhuri, N. R. *Inorg. Chim. Acta* **2005**, *358*, 957.

(23) Dong, W.; Wang, Q. L.; Liu, Z. Q.; Liao, D. Z.; Jiang, Z. H.; Yan, S. P.; Cheng, P. *Polyhedron* **2003**, *22*, 3315.

(24) (a) Wang, Z. M.; Luo, J.; Sun, B. W.; Yan, C. H.; Gao, S.; Liao, C. S. *Acta Crystallogr., Sect. C* **2000**, *56*, 786. (b) Luo, J. H.; Hong, M. C.; Weng, J. B.; Zhao, Y. J.; Cao, R. *Inorg. Chim. Acta* **2002**, *329*, 59.

(25) (a) Wu, A. Q.; Zheng, F. K.; Cai, L. Z.; Guo, G. C.; Huang, J. S. *Chin. J. Struct. Chem.* **2004**, *23*, 1143.

(26) Luo, J. H.; Hong, M. C.; Cao, R.; Liang, Y. G.; Zhao, Y. J.; Wang, R. H.; Weng, J. B. *Polyhedron* **2002**, *21*, 893.

(27) Luo, J.; Zhou, X. G.; Gao, S.; Weng, L. H.; Shao, Z. H.; Zhang, C. M.; Li, Y. R.; Zhang, J.; Cai, R. F. *Inorg. Chem. Commun.* **2004**, *7*, 669.

(28) Lin, H. H.; Mohanta, S.; Lee, C. J.; Wei, H. H. *Inorg. Chem.* **2003**, *42*, 1584.

(29) (a) Sun, H. L.; Gao, S.; Ma, B. Q.; Su, G.; Batten, S. R. *Cryst. Growth Des.* **2005**, *5*, 269. (b) Manson, J. L.; Gu, J. Y.; Schlueter, J. A.; Wang, H. H. *Inorg. Chem.* **2003**, *42*, 3950. (c) Jensen, P.; Batten, S. R.; Moubaraki, B.; Murray, K. S. *J. Chem. Soc., Dalton Trans.* **2002**, 3712. (d) Triki, S.; Thetiot, F.; Galán-Mascarós, J. R.; Pala, J. S. *New J. Chem.* **2001**, *25*, 954. (e) Jensen, P.; Batten, S. R.; Moubaraki, B.; Murray, K. S. *J. Solid State Chem.* **2001**, *159*, 352.

(30) Martin, S.; Barandika, M. G.; de Larramendi, J. I. R.; Cortes, R.; Font-Bardia, M.; Lezama, L.; Serna, Z. E.; Solans, X.; Rojo, T. *Inorg. Chem.* **2001**, *40*, 3687.

Compounds of formula $[M(dca)_2(phen)]_n$ [M = Mn (**1**), Cu (**13**), Zn (**14**), and Cd(II) (**15**)] have been previously characterized from both structural (**1**, **13**−**15**) and magnetic (**1** and **13**) points of view.[19,23−26] These four compounds are isostructural, the structure consisting of (6,3) buckled sheets formed by dca anions which act both as single and double μ-1,5-bridges. Interestingly, the magnetic coupling in **13** is ferromagnetic ($J = +0.2$ cm^{-1}),[19,24b] whereas that in **1** is antiferromagnetic ($J = -1.3$ cm^{-1}).[23] The magnetic properties of this last compound were investigated only in the high-temperature range (77−300 K).

The present work focuses on ways to modify the network topology, and consequently, the magnetic properties of extended systems with dca bridges by subtle variations of the co-ligand. Here, we show the magneto-structural results that we have obtained when using 1,10-phenanthroline (phen) [**1**−**4**] and two of its derivatives, namely, 4,7-dimethylphenanthroline (4,7-dmphen) [**5**−**8**] and 2,9-dimethylphenanthroline (2,9-dmphen) [**9**−**12**], as auxiliary ligands (L) in dca complexes of formula $[M(dca)_2L]_n$ with M = Mn(II) (**1**, **5**, and **9**), Fe(II) (**2**, **6**, and **10**), Co(II) (**3**, **7**, and **11**), and Ni(II) (**4**, **8**, and **12**).

Experimental Section

Materials. All the reagents were purchased from Aldrich and used without further purification. Elemental analysis (C, H, N) were carried out by the Microanalytical Service of the Università della Calabria (Italy).

Preparations. $[Mn(dca)_2(phen)]_n$ (1). Single crystals of **1** were prepared by using $MnCl_2\cdot 4H_2O$ instead of $Mn(ClO_4)_2\cdot 6H_2O$ as previously described.[23] Phen (0.1 mmol, 0.018 g) was dissolved in a minimum amount of ethanol and added to an aqueous solution containing $MnCl_2\cdot 4H_2O$ (0.2 mmol, 0.040 g) and Na(dca) (0.4 mmol, 0.036 g). Slow evaporation at room temperature gave light yellow crystals of **1**. Yield: ca. 50%. Anal. Calcd for $C_{16}H_8MnN_8$ (**1**): C, 52.3; H, 2.2; N, 30.5. Found: C, 52.12; H, 2.32; N, 30.66. IR data on KBr (ν, cm^{-1}) pellets: 2301s $\nu_s + \nu_{as}$(C≡N), 2252s ν_{as}(C≡N), 2175s ν_s (C≡N), 1370 ν_{as}(C−N), 930 ν_s(C−N).

$[Fe(dca)_2(phen)]_n$ (2). Aqueous solutions of $FeCl_2\cdot 4H_2O$ (0.2 mmol, 0.040 g dissolved in 3 cm^3 of solvent) and Na(dca) (0.4 mmol, 0.036 g dissolved in 1 cm^3 of solvent) were mixed, introduced into a 2 cm tube, and layered with water. The resulting solution was first layered with pure ethanol (15 cm^3) and then with an ethanolic solution of phen (0.1 mmol, 0.018 g dissolved in 3 cm^3 of ethanol). The reaction mixture was stoppered and allowed to diffuse at room temperature. Cubic red crystals of **1** were formed after several days. Yield: ca. 60%. Anal. Calcd for $C_{16}H_8FeN_8$ (**2**): C, 58.20; H, 2.19; N, 30.44. Found: C 58.80; H, 2.25; N, 29.72. IR data on KBr (ν, cm^{-1}) pellets: 2305s $\nu_s + \nu_{as}$(C≡N), 2242s ν_{as}(C≡N), 2152s ν_s (C≡N), 1373 ν_{as}(C−N), 922 ν_s(C−N).

$[Co(dca)_2(phen)]_n$ (3). Phen (0.1 mmol, 0.018 g), dissolved in a minimum amount of ethanol, was added to an aqueous solution containing $CoCl_2\cdot 6H_2O$ (0.2 mmol, 0.048 g) and Na(dca) (0.4 mmol, 0.036 g). Small pink chunky crystals of **2** were grown after 2 days. X-ray quality crystals of this compound were obtained by slow diffusion in a manner analogous to that for compound **2** over a period of 1 month. Yield: ca. 40%. Anal. Calcd for $C_{16}H_8CoN_8$ (**3**): C, 51.77; H, 2.17; N, 30.19. Found: C, 52.01; H, 2.30; N, 29.44. IR data on KBr (ν, cm^{-1}) pellets: 2298s $\nu_s + \nu_{as}$(C≡N), 2248s ν_{as}(C≡N), 2175s ν_s (C≡N), 1367 ν_{as}(C−N), 925 ν_s(C−N).

$[Ni(dca)_2(phen)]_n$ (4). X-ray quality light blue parallelepipeds of **4** were obtained in a manner analogous to that for **2** using $NiCl_2\cdot 6H_2O$. Yield: ca. 50%. Anal. Calcd for $C_{16}H_8NiN_8$ (**4**): C, 51.80; H, 2.17; N, 30.20. Found: C, 52.65; H, 2.32; N, 29.70. IR data on KBr (ν, cm^{-1}) pellets: 2302s $\nu_s + \nu_{as}$(C≡N), 2244 ν_{as}(C≡N), 2164s ν_s (C≡N), 1370 ν_{as}(C−N), 945 ν_s(C−N).

$[Mn(dca)_2(4,7\text{-dmphen})]_n$ (5). Slow diffusion of an ethanolic solution of 2,9-dmphen (0.1 mmol, 0.021 g) into an aqueous solution containing of $MnCl_2\cdot 4H_2O$ (0.2 mmol, 0.040 g) and Na(dca) (0.4 mmol, 0.036 g) gave a mixture of light yellow needles of a mononuclear compound of formula $[Mn(dca)_2(4,7\text{-dmphen})_2]$ (**5a**) (ca. 30% yield) and yellow rhombohedral crystals of **5** (ca. 40% yield). The two types of crystals were manually separated and analyzed by X-ray diffractometry. Anal. Calcd for $C_{18}H_{12}MnN_8$ (**5**): C, 54.69; H, 3.06; N, 28.35. Found: C, 55.32; H, 2.99; N, 27.95. Anal. Calcd for $C_{32}H_{24}MnN_{10}$ (**5a**): C, 63.68; H, 4.01; N, 23.21. Found: C, 63.86; H, 3.94; N, 23.70. IR data for compound **5** on KBr (ν, cm^{-1}) pellets: 2300s $\nu_s + \nu_{as}$(C≡N); 2265s ν_{as}(C≡N); 2179s ν_s (C≡N); 1360 ν_{as}(C−N), 922 ν_s(C−N).

$[Fe(dca)_2(4,7\text{-dmphen})]_n$ (6). X-ray quality crystals of **6** as red plates were obtained by slow diffusion of an ethanolic solution of 2,9-dmphen (0.1 mmol, 0.021 g) into an aqueous solution containing of $FeCl_2\cdot 4H_2O$ (0.2 mmol, 0.040 g) and Na(dca) (0.4 mmol, 0.036 g). Yield: ca. 50%. Anal. Calcd for $C_{18}H_{12}FeN_8$ (**6**): C, 54.57; H, 3.05; N, 28.28. Found: C, 55.18; H, 3.00; N, 28.10. IR data on KBr (ν, cm^{-1}) pellets: 2295s $\nu_s + \nu_{as}$(C≡N), 2259s ν_{as}(C≡N), 2171s ν_s (C≡N), 1360 ν_{as}(C−N), 939 ν_s(C−N).

$[Co(dca)_2(4,7\text{-dmphen})]_n$ (7). X-ray quality crystals of **7** as red cubes were obtained by following the procedure described for **6** but using $CoCl_2\cdot 6H_2O$ instead of $FeCl_2\cdot 4H_2O$. Yield: ca. 40%. Anal. Calcd for $C_{18}H_{12}CoN_8$ (**7**): C, 54.15; H, 3.03; N, 28.06. Found: C, 54.35; H, 2.99; N, 28.22.7. IR data on KBr (ν, cm^{-1}) pellets: 2305s $\nu_s + \nu_{as}$(C≡N), 2260s ν_{as}(C≡N), 2170s ν_s (C≡N), 1372 ν_{as}(C−N), 930 ν_s(C−N).

$[Ni(dca)_2(4,7\text{-dmphen})]_n$ (8). The same procedure described for **6**, but using $NiCl_2\cdot 6H_2O$ instead of $FeCl_2\cdot 4H_2O$, yielded turquoise chunky crystals (**8a**, ca. 30% yield), together with a majority of purple thin plates crystals (compound **8**, ca. 50% yield). The two compounds were separated by hand. Anal. Calcd for $C_{18}H_{12}NiN_8$ (**8**): C, 54.18; H, 3.03; N, 28.08. Found: C, 54.32; H, 2.98; N, 28.27. IR data on KBr (ν, cm^{-1}) pellets: 2301s $\nu_s + \nu_{as}$(C≡N), 2245s ν_{as}(C≡N), 2155s ν_s (C≡N), 1345 ν_{as}(C−N), 950 ν_s(C−N).

Crystals of **8a** were too small and diffract very poorly to perform structure determination. The quick loss of crystallinity in **8a** moved us to perform thermogravimetric analysis that confirm the presence of a half water molecule for a compound of formula $[Ni(dca)_2(4,7\text{-dmphen})]_n\cdot 0.5nH_2O$. Anal. Calcd for $C_{18}H_{13}NiN_8O_{0.5}$ (**8a**): C, 52.98; H, 3.21; N, 27.46. Found: C, 53.50; H, 3.02; N, 28.05. IR data on KBr (ν, cm^{-1}) pellets: 2305s $\nu_s + \nu_{as}$(C≡N), 2239s ν_{as}(C≡N), 2148s ν_s (C≡N), 1350 ν_{as}(C−N), 910 ν_s(C−N), 3580s,br, 3170s,br (H_2O).

$[Mn(dca)_2(2,9\text{-dmphen})]_n$ (9). Na(dca) (0.2 mmol, 0.018 g) dissolved in the minimum amount of water was added to an aqueous solution of $MnCl_2\cdot 4H_2O$ (0.1 mmol, 0.020 g). An ethanolic solution of 2,9-dmphen (0.1 mmol, 0.021 g) was added to this solution, and the resulting mixture was gently warmed during fifteen minutes. Yellow droplike crystals of **9** were separated in a couple of days by slow evaporation of the resulting solution at room temperature. Yield: ca. 50%. Anal. Calcd for $C_{18}H_{12}MnN_8$ (**9**): C, 54.69; H, 3.06; N, 28.35. Found: C, 54.95; H, 2.85; N, 28.10. IR data on KBr (ν, cm^{-1}) pellets: 2302s $\nu_s + \nu_{as}$(C≡N), 2262s ν_{as}(C≡N), 2165s ν_s (C≡N), 1365 ν_{as}(C−N), 920 ν_s(C−N).

Table 1. Crystal Data and Structure Refinement for Compounds **1**−**8**[a]

	1	**2**	**3**	**4**	**5**	**6**	**7**	**8**
empirical formula	$C_{16}H_8MnN_8$	$C_{16}H_8FeN_8$	$C_{16}H_8CoN_8$	$C_{16}H_8NiN_8$	$C_{18}H_{12}MnN_8$	$C_{18}H_{12}FeN_8$	$C_{18}H_{12}CoN_8$	$C_{18}H_{12}NiN_8$
fw	367.24	368.15	371.23	371.01	395.30	396.21	399.29	399.07
a (Å)	10.161(2)	10.1388(6)	10.1071(8)	10.0591(2)	11.023(1)	10.9810(3)	10.9540(6)	10.9540(6)
b (Å)	10.935(2)	10.9373(7)	10.9569(9)	10.9889(2)	11.474(1)	11.4061(3)	11.4147(6)	11.4147(6)
c (Å)	14.407(3)	14.2059(7)	14.128(1)	14.0219(3)	14.113(1)	13.9694(4)	13.9354(7)	13.9354(7)
β (deg)	100.62(3)	101.062(2)	101.257(3)	101.384(1)	100.633(3)	101.421(1)	101.660(1)	101.660(1)
V (Å^3)	1573.3(5)	1546.0(2)	1534.5(2)	1519.47(5)	1754.3(3)	1715.03(8)	1706.5(2)	1706.5(2)
D_c (g cm^{-3})	1.550	1.582	1.607	1.622	1.497	1.534	1.554	1.553
μ (mm^{-1})	0.856	0.992	1.135	1.294	0.773	0.901	1.027	1.158
[b]R1 [$I > 2\sigma(I)$]	0.0321	0.0280	0.0293	0.0314	0.0316	0.0337	0.0397	0.0308
[c,d]wR2	0.0907	0.0793	0.0827	0.0914	0.0835	0.0915	0.1123	0.0851

[a] Details in common: monoclinic, $P2_1/c$, $T = 293(2)$ K, and $Z = 4$. [b] $R1 = \sum||F_o| - |F_c||/\sum|Fo|$. [c] $wR2 = \{\sum[w(F_o^2 - F_c^2)^2]/[(w(F_o^2)^2]\}^{1/2}$. [d] $w = 1/[\sigma^2(F_o^2) + (aP)^2 + bP]$ with $P = [F_o^2 + 2F_c^2]/3$, $a = 0.0520$ (**1**), 0.0434 (**2**), 0.0464 (**3**), 0.0533 (**4**), 0.0477 (**5**), 0.0625 (**6**), 0.0681 (**7**), and 0.0431(**8**) and $b = 0.2331$ (**1**), 0.1663 (**2**), 0.2247 (**3**), 0.1845 (**4**), 0.3340 (**5**), 0.1009 (**6**), 0.0000 (**7**), and 0.5609 (**8**).

[Fe(dca)$_2$(2,9-dmphen)]$_n$ (10). An ethanolic solution of 2,9-dmphen (0.1 mmol, 0.021 g dissolved in 1 cm^3 of solvent) was added to an aqueous solution of $FeCl_2 \cdot 4\ H_2O$ (0.2 mmol, 0.020 g) and Na(dca) (0.4 mmol, 0.036 g). The small amount of precipitate which appeared was removed by filtration, and the clear solution was left to evaporate in the open air at room temperature. Red polyhedra of **10** were formed after 4 days. They were suitable for X-ray diffraction. Yield: ca. 65%. Anal. Calcd for $C_{18}H_{12}FeN_8$ (**10**): C, 54.57; H, 3.05; N, 28.28. Found: C, 54.89; H, 2.98; N, 28.10. IR data on KBr (ν, cm^{-1}) pellets: 2309s $\nu_s + \nu_{as}$(C≡N), 2246s ν_{as}(C≡N), 2164s ν_s (C≡N), 1349 ν_{as}(C−N), 918 ν_s(C−N).

[Co(dca)$_2$(2,9-dmphen)]$_n$ (11). 2,9-dmphen (0.1 mmol, 0.021 g), dissolved in 1 cm^3 of ethanol, was added dropwise to an aqueous solution containing $CoCl_2 \cdot 6H_2O$ (0.2 mmol, 0.048 g) and Na(dca) (0.4 mmol, 0.036 g). The reaction mixture was stirred during 30 min and then filtered. Well shaped mauve polyhedral crystals of **11** were obtained from the mother liquor by slow evaporation at room temperature after 3 days. They were filtered, washed with a small amount of water, and air-dried. Yield: ca. 50%. Anal. Calcd for $C_{18}H_{12}CoN_8$ (**11**): C, 54.15; H, 3.03; N, 28.06. Found: C, 54.40; H, 2.91; N, 27.87. IR data on KBr (ν, cm^{-1}) pellets: 2300s $\nu_s + \nu_{as}$(C≡N), 2243s ν_{as}(C≡N), 2160s ν_s (C≡N), 1365 ν_{as}(C−N), 925, ν_s(C−N).

[Ni(dca)$_2$(2,9-dmphen)]$_n$ (12). Compound **12** was prepared by following a procedure similar to that described for complex **3** but using 2,9-dmphen instead of phen. Complex **12** was obtained as sky blue parallelepipeds which were filtered, washed with water, and air-dried. Yield: ca. 40%. Anal. Calcd for $C_{18}H_{12}NiN_8$ (**12**): C, 54.18; H, 3.03; N, 28.08. Found: C, 54.42; H, 3.00; N, 27.87. IR data on KBr (ν, cm^{-1}) pellets: 2300s $\nu_s + \nu_{as}$(C≡N), 2260s ν_{as}(C≡N), 2165s ν_s (C≡N), 1363 ν_{as}(C−N), 925 ν_s(C−N).

Physical Techniques. IR spectra were recorded on a Perkin-Elmer 1750 FTIR spectrophotometer as KBr pellets in the 4000−400 cm^{-1} region. Magnetic susceptibility measurements of polycrystalline samples of **1**−**12** were performed in the temperature range of 1.9−290 K with a Quantum Design SQUID susceptometer, using an applied field of 1000 G. $(NH_4)_2Mn(SO_4)_2 \cdot 6H_2O$ was used as a susceptibility standard. The independence of the magnetic measurements on the applied magnetic field was checked for the samples with M = Ni which exhibit ferromagnetic coupling. The magnetization versus H plots were carried out at 2.0 K in the 0−5 T field range. Diamagnetic corrections of the constituent atoms were estimated from Pascal constants[31] and found to be -199.4×10^{-6} (**1**), -198.4×10^{-6} (**2**), -197.4×10^{-6} (**3** and **4**), -221.1×10^{-6} (**5** and **9**), -220.1×10^{-6} (**6** and **10**), and -219.1×10^{-6} cm^3 mol^{-1} (**7**, **8**, **11**, and **12**). Corrections for the temperature-independent paramagnetism (TIP) of the metal ions, as well as for the sample holder, were also applied.

Table 2. Crystal Data and Structure Refinement for Compounds **9**−**12**[a]

	9	**10**	**11**	**12**
empirical formula	$C_{18}H_{12}MnN_8$	$C_{18}H_{12}FeN_8$	$C_{18}H_{12}CoN_8$	$C_{18}H_{12}NiN_8$
fw	395.30	396.21	399.29	399.07
a (Å)	8.876(2)	8.8877(4)	8.8604(2)	8.8725(4)
b (Å)	15.640(3)	15.5110(7)	15.4093(3)	15.3131(7)
c (Å)	12.980(3)	12.9489(6)	12.8625(2)	12.8028(6)
β (Å)	94.39(3)	94.887(2)	94.493(1)	93.926(2)
V (Å^3)	1796.6(6)	1778.61(14)	1750.75(6)	1735.38(14)
D_c (g cm^{-3})	1.461	1.480	1.515	1.527
μ (mm^{-1})	0.755	0.868	1.001	1.139
[a]R1 [$I > 2\ \sigma\ (I)$]	0.0654	0.0408	0.0336	0.0334
[b,c]wR2	0.1416	0.1246	0.0975	0.1012

[a] Details in common: monoclinic, $P2_1/n$, $T = 293(2)$ K, and $Z = 4$. [b] $R1 = \sum||F_o| - |F_c||/\sum|F_o|$. [c] $wR2 = \{\sum[w(F_o^2 - F_c^2)^2]/[(w(Fo^2)^2]\}^{1/2}$. [d] $w = 1/[\ \sigma^2(F_o^2) + (aP)^2 + bP]$ with $P = [F_o^2 + 2F_c^2]/3$, $a = 0.0816$ (**9**), 0.0864 (**10**), 0.0607 (**11**), and 0.0633 (**12**) and $b = 0.0000$ (**9**), 0.0000 (**10**), 0.3602 (**11**), and 0.1512 (**12**).

X-ray Data Collection and Structure Refinement. X-ray diffraction data were collected using a Bruker R3m/V automatic four-circle for compound **9** and a Bruker-Nonius X8 APEXII CCD area detector diffractometer for the other complexes. Graphite-monochromated Mo Kα radiation ($\lambda = 0.71073$ Å) was used in both cases. Lorentz-polarization and empirical absorption corrections through the ψ-scan program[32] were applied for compound **9**. The data for compounds **2**−**8** and **10**−**12** were processed through the SAINT[33a] reduction and SADABS[33b] absorption software. The structures were solved by direct methods and subsequently completed by Fourier recycling using the SHELXTL software package.[34] Non-hydrogen atoms were refined anisotropically. Hydrogen atoms were set in calculated positions and refined as riding atoms. Full-matrix least-squares refinements on F^2, carried out by minimizing the function $\sum w(|F_o| - |F_c|)^2$, reached convergence with values of the discrepancy indices given in Tables 1 and 2. The final geometrical calculations were carried out with the PARST program.[35] The graphical manipulations were performed using the XP utility of the SHELXTL system. Crystallographic data are listed in Tables 1 (**1**−**8**) and 2 (**9**−**12**). Selected bond lengths and angles

(31) Earnshaw, A. *Introduction to Magnetochemistry*; Academic Press: London, 1968.
(32) North, A. C. T.; Philips, D. C.; Mathews, F. S. *Acta Crystallogr., Sect A* **1968**, *24*, 351.
(33) (a) *SAINT*, version 6.45; Bruker Analytical X-ray Systems Inc.: Madison, WI, 2003. (b) Sheldrick, G. M. *SADABS Program for Absorption Correction*, version 2.10; Analytical X-ray Systems: Madison, WI, 2003.
(34) *SHELXTL*; Bruker Analytical X-ray Instruments: Madison, WI, 1998
(35) Nardelli, M. *Comput. Chem.* **1983**, *7*, 95.

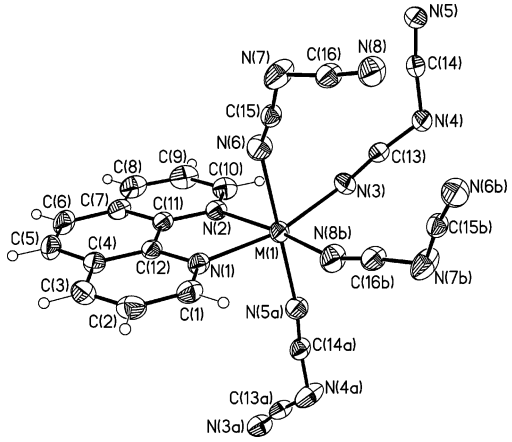

Figure 1. Perspective view of the asymmetric unit for compounds of formula $[M(dca)_2(phen)]_n$, where M = Fe (**2**), Co (**3**), and Ni (**4**), showing the atom numbering scheme. Thermal ellipsoids are shown at the 30% probability level.

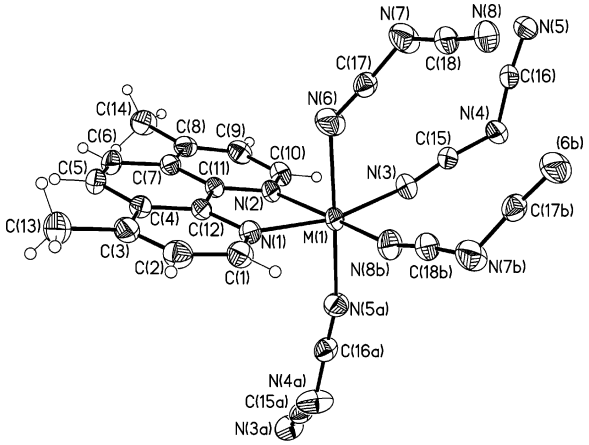

Figure 2. Perspective view of the asymmetric unit for compounds of formula $[M(dca)_2(4,7\text{-dmphen})]_n$, where M = Mn (**5**), Fe (**6**), Co (**7**), and Ni (**8**), showing the atom numbering scheme. Thermal ellipsoids are shown at the 30% probability level.

around the metal atoms are given in Tables 3 (**1**−**8**) and 4 (**9**−**12**), while structural data concerning the dca ligands [Tables S1 and S2 (**2**−**12**)] and the intralayer metal−metal separations [Table S3 (**2**−**8**) and S4 (**9**−**12**)] are given as Supporting Information. CCDC reference numbers are 293564−293574 for complexes **2**−**12**, respectively.

Results and Discussion

Infrared Spectra. The IR spectra of compounds **2**−**12** are quite similar, as shown in the Experimental Section, their profiles being determined to a large extent by the dca ligand. They all show strong absorptions in the 2310−2100 cm^{-1} region, corresponding to the $\nu_s + \nu_{as}(C{\equiv}N)$, $\nu_{as}(C{\equiv}N)$, and $\nu_s(C{\equiv}N)$ modes of the dca ligand.[36] The shift toward higher frequencies of these peaks, when compared with those of the free dca in its sodium salt (strong peaks at 2286, 2232, and 2129 cm^{-1}), is consistent with the coordination of the ligand. Bands from the $\nu_{as}(C-N)$ (1400−1300 cm^{-1}) and $\nu_s(C-N)$ (950−900 cm^{-1}) vibrations also occur in the spectra of **2**−**12**.

Description of the Structures of 2−8. Compounds **2**−**8** are isostructural to each other and also to the $[M(dca)_2(phen)]$ compounds [M = Mn (**1**), Cu (**13**), Zn (**14**), and Cd (**15**)].[23−26]

Each metal ion in **2**−**8** is six-coordinated: two nitrogen atoms [N(1) and N(2)] of the phen (**2**−**4**) or 4,7-dmphen (**5**−**8**) groups and two nitrogen atoms [N(3) and N(8b); symmetry code b = $-x$, $-y$, $1 - z$] of two dca ligands in the equatorial positions, together with two other two nitrogen atoms [N(6) and N(5a); symmetry code a = x, $0.5 - y$, $0.5 + z$] of the remaining dca ligands in the axial positions build a distorted MN_6 octahedral environment. The metal surroundings of compounds **2**−**4** and **5**−**8** are shown in Figures 1 and 2, respectively. The reduced value of the bite angle of the chelating ligand [the values of the N(1)−M−N(2) angle vary between 73.10(5)° (**5**) and 79.95(5)° (**4**)] is the main factor accounting for the distortion of the metal environment from the ideal octahedral geometry.

Each metal atom is connected to the other three metal centers by means of two single and one double dca bridges, in an end-to-end ($\mu_{1,5}$) coordination mode, leading to layers which grow in the *bc* plane. As a result, the topology of the coordination network is that of a herringbone-waved grid because the rings have a slight chair conformation [see Figures 3 (**2**−**4**) and S1 (**5**−**8**)]. The bidentate phen and 4,7-dmphen ligands are located on both sides of each layer. The layers are connected through stacking interactions between the aryl rings of the phenanthroline moiety, each one being parallel to an equivalent one in the adjacent layer. The average distances between the average phenanthroline planes are 3.39 and 3.45 Å in **2**−**4** and **5**−**8**, respectively. The single dca bridges are cis to each other, the mean value of the N(3)−M(1)−N(5a) angle being 95.96°. The values of the M···M distance through the double dca bridge vary between 7.2571(3) and 7.3820(4) Å in **2**−**4** and between 7.2990(4) and 7.3661(6) Å in **5**−**8**, and they are always shorter than those distances through the single dca bridge [7.6017(3)−7.6639(4) (**2**−**4**) and 7.9326(3)−8.0406(6) Å (**5**−**8**)] (see Table S3).

A greater shift of the metal ion from the equatorial plane in the compounds containing 4,7-dmphen (**5**−**8**) [maximum and minimum values being 0.183(1) and 0.127(1) Å in compounds **5** and **8**, respectively] is observed when compared to those with the phen group (**2**-**4**) [maximum and minimum values being 0.131(1) (**2**) and 0.098(1) Å (**4**)]. The aromatic skeleton of the phen/4,7-dmphen is almost planar in all the compounds, but larger deviations from planarity can be observed in the phen series. So, the maximum deviation from planarity in the phen series is 0.030(2) Å (**4**) to be compared with the maximum value in the 4,7-dmphen family of 0.009(1) Å (**8**). Bond lengths and angles of the coordinated phen and 4,7-dmphen agree well with those observed in the free phen molecule.[37]

(36) Köhler, H.; Kolbe, A.; Lux, G. *Z. Anorg. Allg. Chem.* **1977**, *428*, 103.

(37) (a) Sen, M. *Acta Crystallogr., Sect. B* **1974**, *30*, 556. (b) Nishigaki, S.; Yoshioka, H.; Nakatsu, K. *Acta Crystallogr., Sect. B* **1975**, *31*, 1220. (c) Tian, Y. P.; Duan, C. Y.; Xu, X. X.; You, X. Z. *Acta Crystallogr., Sect. C* **1995**, *51*, 2309. (d) Ng, S. W. *Z. Krystallogr.−New Cryst. Struct.* **1997**, *212*, 283.

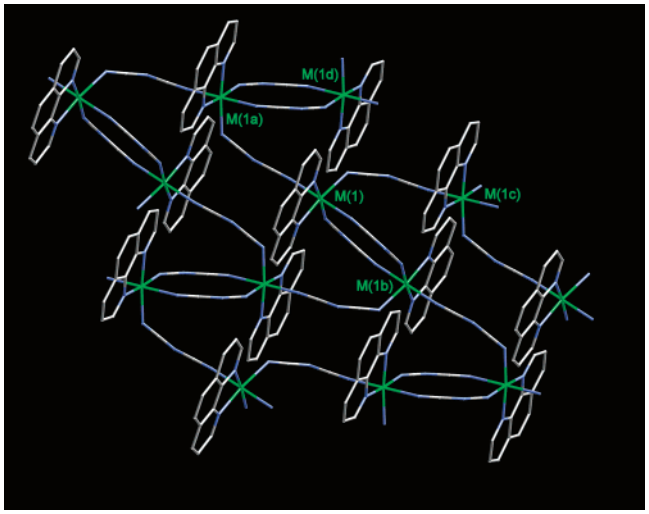

Figure 3. Perspective view of the 2D herringbone grid of frameworks **2** (M = Fe), **3** (M = Co), and **4** (M = Ni) lying in the crystallographic *ab* plane.

The angles subtended at the amide nitrogen atom vary in the range 119.8(2)−120.2(2)° (**2**−**8**) in the double dca bridges, whereas the mean values of 122.2(2) (**2**−**4**) and 124.5(2)° (**5**−**8**) are observed in the single dca bridges. Nitrile and amide carbon−nitrogen distances in the dca groups cover the ranges of 1.132(2)−1.158(2) and 1.280(2)−1.314(2) Å, respectively (see Tables S1 and S2). These values are consistent with the triple and single carbon−nitrogen bond character, and they are in agreement with those observed in other complexes where dca features the end-to-end coordination mode.[1,8−14,16−30]

Description of the Structures of 9−12. Compounds **9**−**12** are isostructural two-dimensional compounds. The chromophore around the metal atom in **9**−**12** is the same as that of **1**−**8**. Each metal ion in **9**−**12** is six-coordinated: two nitrogen atoms of the chelating 2,9-dmphen ligand [N(1) and N(2)], two nitrogen atoms from dca anions [N(6) and N(8b); symmetry code b = $-x$, $2-y$, $2-z$] in the equatorial positions, and other two nitrogen atoms from two other dca groups [N(3) and N(5a); symmetry code a = $0.5-x$, $0.5+y$, $1.5-z$] in the axial positions build a distorted octahedral surrounding (see Figure 4). The reduced value of the angle subtended at the metal atom by the bidentate 2,9-dmphen ligand [values of N(1)−M(1)−N(2) varying in the range of 72.8(2)−78.92(5)°] and the steric hindrance of the methyl substituents are most likely responsible for the distortion of the coordination sphere of the metal atoms in **9**−**12**. In particular, the values of the $M-N_{(2,9-dmphen)}$ bond lengths in **9**−**12** are longer than those with the phen (**1**−**4**) and 4,7-dmphen (**5**−**8**) compounds.

The dca anions show the end-to-end ($\mu_{1,5}$) coordination mode forming both single and double bridges between the metal centers. A layered structure occurs also in **9**−**12**, but the arrangement of the metal atoms in each layer here (Figure 5) is different from that found in **1**−**8**. This is the result of the single dca bridges in **9**−**12** being in trans positions [the values of the N(3)−M(1)−N(5a) angles vary in the range of 176.63(7)−177.59(7)°]. These bridges build chains growing along the *b* axis. The other two dca anions coordinated

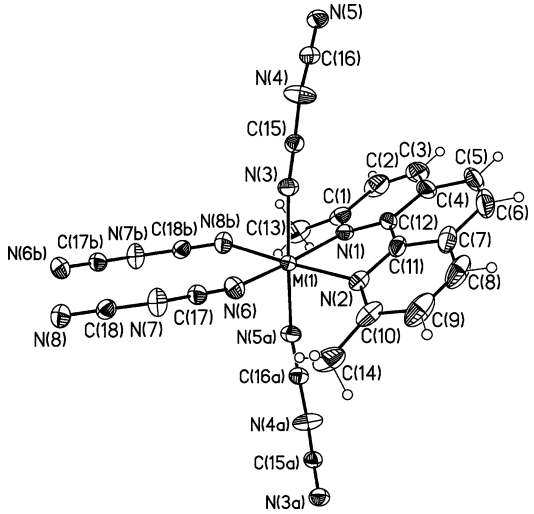

Figure 4. Perspective view of the asymmetric unit for compounds of formula $[M(dca)_2(2,9\text{-dmphen})]_n$, where M = Mn (**9**), Fe (**10**), Co (**11**), and Ni (**12**), showing the atom numbering scheme. Thermal ellipsoids are shown at the 30% probability level.

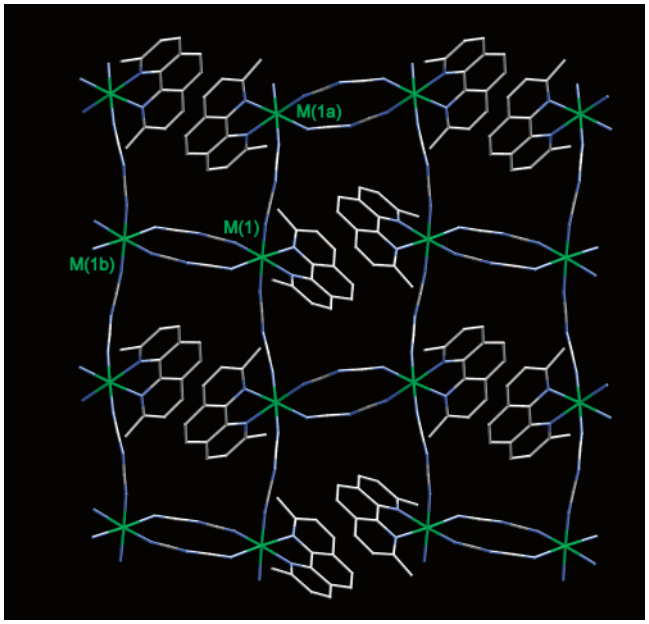

Figure 5. Perspective view of the (6,3) grid of frameworks **9** (M = Mn), **10** (M = Fe), **11** (M = Co), and **12** (M = Ni) showing the stacking interactions between 2,9-dmphen ligands.

to each metal center connect it to another metal atom by means of a double dca bridge, giving rise to the layer. The 2,9-dmphen ligands are not coplanar with the equatorial planes (most likely because of steric effects between the methyl groups), and they form a dihedral angle whose value varies between 27.9(1) (**12**) and 30.1(1)° (**9**). The metal ion in this family of compounds is less shifted from the mean equatorial plane compared to that in **2**−**8**, the maximum and minimum deviations being 0.124(1) and 0.090(1) Å in **9** and **12**, respectively. Intralayer $\pi-\pi$ stacking between the phenanthroline rings occurs in **9**−**12**, the distances between the mean planes in each pair of 2,9-phen molecules ranging from 3.53 to 3.55 Å (Figure 5). In contrast to what is found in the phen- and 4,7-dmphen-containing compounds, no $\pi-\pi$ stacking between adjacent layers occurs in **9**−**12**. The 2,9-

Table 3. Selected Bond Distances (Å) and Angles (deg) for Compounds **1**−**8**[a,b]

M	Mn (**1**)	Fe (**2**)	Co (**3**)	Ni (**4**)	Mn (**5**)	Fe (**6**)	Co (**7**)	Ni (**8**)
M(1)−N(1)	2.2666(14)	2.1797(13)	2.1344(14)	2.0851(14)	2.2511(13)	2.1744(14)	2.1268(14)	2.0798(15)
M(1)−N(2)	2.2484(15)	2.1657(12)	2.1209(13)	2.0715(12)	2.2708(13)	2.1871(13)	2.1358(13)	2.0947(14)
M(1)−N(3)	2.1998(17)	2.1435(15)	2.1346(16)	2.1068(16)	2.1695(16)	2.1143(17)	2.0968(18)	2.0767(18)
M(1)−N(6)	2.3288(17)	2.2531(15)	2.2109(16)	2.1570(15)	2.3625(17)	2.2878(18)	2.263(2)	2.2090(18)
M(1)−N(5a)	2.1932(15)	2.1470(14)	2.1085(14)	2.0777(14)	2.1798(14)	2.1295(15)	2.0988(16)	2.0803(16)
M(1)−N(8b)	2.1619(17)	2.1070(14)	2.0845(15)	2.0508(14)	2.1859(16)	2.1244(15)	2.0958(16)	2.0750(16)
N(1)−M(1)−N(2)	73.55(5)	76.48(5)	78.06(5)	79.95(5)	73.10(5)	75.56(5)	77.43(5)	78.96(6)
N(1)−M(1)−N(3)	164.09(6)	166.72(5)	167.95(5)	169.74(5)	163.29(6)	165.13(6)	166.71(6)	168.81(6)
N(1)−M(1)−N(6)	82.56(6)	84.44(5)	84.65(6)	85.70(6)	82.58(6)	83.29(6)	83.59(7)	84.90(7)
N(1)−M(1)−N(5a)	96.33(6)	95.13(5)	95.28(6)	94.10(6)	95.95(6)	95.49(6)	94.92(6)	93.60(6)
N(1)−M(1)−N(8b)	93.82(7)	93.36(6)	94.61(6)	94.15(6)	92.00(6)	91.87(6)	92.68(6)	93.13(7)
N(2)−M(1)−N(3)	97.69(6)	96.15(6)	96.26(6)	95.29(6)	95.39(6)	94.87(6)	95.29(7)	95.03(7)
N(2)−M(1)−N(6)	86.13(6)	89.21(5)	89.13(5)	89.46(5)	86.77(5)	87.64(6)	87.46(6)	88.22(6)
N(2)−M(1)−N(5a)	91.42(5)	91.05(5)	90.70(5)	90.61(5)	92.18(5)	92.15(5)	91.86(6)	91.43(6)
N(2)−M(1)−N(8b)	166.98(7)	169.69(6)	172.53(6)	173.99(6)	164.39(6)	166.68(6)	169.24(6)	171.25(7)
N(3)−M(1)−N(6)	83.63(6)	84.43(6)	84.64(6)	85.18(6)	84.74(7)	84.99(7)	85.00(8)	85.50(8)
N(3)−M(1)−N(5a)	97.16(6)	96.05(6)	95.42(6)	95.03(6)	96.58(6)	96.23(7)	96.43(7)	95.99(7)
N(3)−M(1)−N(8b)	93.82(7)	93.47(6)	90.67(7)	90.35(7)	98.10(7)	96.52(7)	93.57(7)	92.14(7)
N(6)−M(1)−N(5a)	177.51(6)	179.43(6)	179.82(6)	179.78(6)	178.39(6)	178.78(7)	178.47(7)	178.50(7)
N(6)−M(1)−N(8b)	89.13(7)	88.04(6)	88.74(6)	88.93(6)	86.67(6)	86.49(6)	87.23(7)	87.36(7)
N(5a)−M(1)−N(8b)	93.17(7)	91.62(6)	91.43(6)	90.98(6)	94.05(6)	93.46(6)	93.21(7)	92.79(7)

[a] Estimated standard deviations in the last significant digits are given in parentheses. [b] Symmetry code: (a) x, $0.5 - y$, $0.5 + z$; (b) $-x$, $-y$, $1 - z$; (c) x, $0.5 - y$, $-0.5 + z$.

dmphen ligand deviates from planarity, with mean deviations spanning in the range of 0.075(6)−0.105(2) Å. Bond distances and angles in the 2,9-dmphen ligand from **9**−**12** agree with those observed in the free 2,9-dmphen molecule.[38]

Bond distances and angles of the dca anions are consistent with the values observed in other complexes featuring this coordination mode.[1,8−14,16−30] These values are similar to those observed in **2**−**8**, with one remarkable exception involving the M−N−C angle: the single dca bridge is bound to the metal ion with mean values for the M(1)−N(3)−C(15) and M(1)−N(5a)−C(16a) angles of 171.2(2) and 160.1(2)°, respectively. The mean values for these angles in compounds **2**−**4** [133.6 and 173.4° for M(1)−N(3)−C(13) and M(1)−N(5a)−C(14a), respectively] and **5**−**8** [151.2(2) and 164.2(2)° for M(1)−N(3)−C(15) and M(1)−N(5a)−C(16a)] show strong deviations form linearity (see Tables S1 and S2).

The values of the M···M distances through the single dca bridge vary in the range of 7.718(1)−7.902(2) Å, while those through the double dca bridge cover the range of 7.389(1)−7.471(1) Å (see Table S4). As observed in the structures of **2**−**8**, the distances through the double dca bridge are shorter, but here the difference between the two values is smaller.

Magnetic Properties of 1−12. The magnetic properties of compounds **1**, **5**, and **9** in the form of $\chi_M T$ versus T plots [χ_M is the magnetic susceptibility per one Mn(II) ion] are shown in Figures 6, 7, and S2, respectively. The $\chi_M T$ value at room temperature for the three compounds is ca. 4.25 cm^3 mol^{-1} K, a value which agrees with the expected for a magnetically isolated spin sextet. Upon cooling, $\chi_M T$ is practically constant until 100 (**1**, **5**) and 50 (**9**) K, and then it gradually decreases to reach 0.70 (**1**), 0.61 (**5**), and 1.38 cm^3 mol^{-1} K (**9**) at 1.9 K. The susceptibility curves [see insets of Figures 5 (**1**), 6 (**5**), and S2 (**9**)] show maxima at 3.2 and 3.5 K for compounds **1** and **5**, respectively, whereas an incipient maximum occurs in **9**. These features are characteristic of a weak antiferromagnetic interaction between the manganese(II) centers. Keeping in mind the honeycomb-layered structure of **1**, **5**, and **9**, where two single and one double μ-1,5 dca bridges define the edges of the repeating hexagonal motif, their magnetic data were analyzed through the theoretical model derived for a two-dimensional Heisenberg classical honeycomb lattice.[39] The best-fit parameters are as follows: $J_1 = -0.017$ cm^{-1}, $J_2 = -0.72$ cm^{-1}, $g = 1.98$, and $R = 8.4 \times 10^{-6}$ for **1**; $J_1 = -0.06$ cm^{-1}, $J_2 = -0.75$ cm^{-1}, $g = 1.98$, and $R = 1.9 \times 10^{-5}$ for **5**; and $J_1 < 10^{-3}$ cm^{-1}, $J_2 = -0.45$ cm^{-1}, $g = 1.99$, and $R = 1.3 \times 10^{-6}$ for **9**. J_1 and J_2 are the exchange interactions through single and double μ-1,5 dca bridges, respectively, g is the Landé factor, and R is the agreement factor defined as $\sum_i[(\chi_M T)_{obsd}(i) - (\chi_M T)_{calcd}(i)]^2/\sum_i[(\chi_M T)_{obsd}(i)]^2$. In a second approach, given that the value of J_1 can be neglected against that of J_2, a fit of the magnetic data of **1**, **5**, and **9** through the expression for a simple manganese(II) dinuclear model [the isotropic Hamiltonian being $\hat{H} = -J_2 S_{Mn(1)} \cdot S_{Mn(2)}$] was performed. Best-fit parameters led to values of J_2 equal to −0.79 (**1**), −0.86 (**5**), and −0.45 cm^{-1} (**9**), the quality of the fit being practically identical to that of the previous ones.

The values of the magnetic coupling in **1** (−0.79 cm^{-1}), **5** (0.86 cm^{-1}), and **9** (−0.45 cm^{-1}) are of the same order than those reported for mixed-ligand Mn(II)/dca/L systems where dca adopts the end-to-end coordination mode, as shown in Table 5. One can see how the magnetic interaction through the single and double end-to-end dca bridges in manganese(II) compounds is always weak and antiferromagnetic, showing the poor ability of the dca ligand in mediating magnetic interactions between paramagnetic metal ions through this bridging mode with metal−metal separations larger than 7.0 Å. MO calculations performed on the

(38) (a) Britton, D.; Thompson, L. C.; Holtz, R. C. *Acta Crystallogr., Sect. C* **1991**, *47*, 1101. (b) Baggio, S.; Baggio, R.; Mombru, A. W. *Acta Crystallogr., Sect. C* **1998**, *54*, 1900.

(39) Curély, J.; Lloret, F.; Julve, M. *Phys. Rev. B* **1988**, *58*, 11465.

Table 4. Selected Bond Distances (Å) and Angles (deg) for Compounds **9**−**12**[a,b]

M	Mn (**9**)	Fe (**10**)	Co (**11**)	Ni (**12**)
M(1)−N(1)	2.281(4)	2.2236(14)	2.1707(15)	2.1282(12)
M(1)−N(2)	2.319(4)	2.2459(16)	2.1884(16)	2.1362(13)
M(1)−N(3)	2.254(5)	2.1796(16)	2.1491(17)	2.1119(13)
M(1)−N(6)	2.186(5)	2.1461(18)	2.1097(18)	2.0750(16)
M(1)−N(5a)	2.168(5)	2.1173(16)	2.0871(18)	2.0584(14)
M(1)−N(8b)	2.198(5)	2.1613(18)	2.1269(18)	2.0953(15)
N(1)−M(1)−N(2)	72.82(16)	75.37(6)	77.09(6)	78.92(5)
N(1)−M(1)−N(3)	82.60(17)	83.40(6)	83.90(6)	84.92(5)
N(1)−M(1)−N(6)	165.38(18)	168.43(7)	169.65(7)	171.36(6)
N(1)−M(1)−N(5a)	95.99(17)	94.59(6)	94.76(7)	94.14(5)
N(1)−M(1)−N(8b)	103.51(18)	102.46(7)	101.29(7)	99.81(6)
N(2)−M(1)−N(3)	87.52(17)	87.25(6)	87.66(7)	87.83(6)
N(2)−M(1)−N(6)	96.37(19)	96.80(7)	96.53(7)	96.04(6)
N(2)−M(1)−N(5a)	90.13(17)	89.62(7)	90.08(7)	90.23(6)
N(2)−M(1)−N(8b)	175.62(18)	176.86(7)	177.01(7)	177.04(6)
N(3)−M(1)−N(6)	87.21(19)	87.78(7)	87.74(7)	87.89(6)
N(3)−M(1)−N(5a)	177.53(18)	176.63(7)	177.59(7)	177.97(6)
N(3)−M(1)−N(8b)	89.64(19)	90.26(7)	89.67(7)	89.39(6)
N(6)−M(1)−N(5a)	93.8(2)	93.84(7)	93.37(7)	92.89(6)
N(6)−M(1)−N(8b)	86.8(2)	85.00(7)	84.71(8)	84.88(6)
N(5a)−M(1)−N(8b)	92.67(18)	92.82(7)	92.57(7)	92.54(6)

[a] Estimated standard deviations in the last significant digits are given in parentheses. [b] Symmetry code: (a) $0.5 - x$, $0.5 + y$, $1.5 - z$; (b) $-x$, $2 - y$, $2 - z$; (e) $0.5 - x$, $-0.5 + y$, $1.5 - z$.

dca ligand and also on dca-bridged manganese(II) dinuclear models[12] have shown very reduced overlaps between the magnetic orbitals through the end-to-end dca bridge, supporting the weak antiferromagnetic interactions observed.

The magnetic properties of compounds **2**, **6**, and **10** in the form of $\chi_M T$ versus T plots [χ_M is the magnetic susceptibility per one Fe(II) ion] are shown in Figure 8. At room temperature, the values of $\chi_M T$ are 3.40 (**2**), 3.30 (**6**), and 3.20 $cm^3\ mol^{-1}$ K (**10**). These values are as expected for a magnetically isolated high-spin iron(II) ion ($S = 2$). Upon cooling, these values remain practically constant until 100 K and then they decrease to reach 0.65 (**2**) and 0.75 $cm^3\ mol^{-1}$ K (**6** and **10**) at 1.9 K. No maximum is observed in the susceptibility versus T plots of these compounds. The decrease of $\chi_M T$ in the low-temperature range for this family of iron(II) compounds is caused by antiferromagnetic interactions through the single and double dca bridges, as observed in the above manganese(II) series. Keeping in mind the results of the analysis of the magnetic data that we performed for **1**, **5**, and **9** (which led us to consider the magnetic coupling through the double dca bridges as the dominant one), we assumed that the magnetic data of **2**, **6**, and **10** can be fitted to a dinuclear model with $\hat{H} = -JS_A \cdot S_B$ ($S_A = S_B = 2$). Best-fit parameters are as follows: $J = -1.25$ cm^{-1}, $g = 2.11$, $\theta = -0.029$ K, and $R = 1.9 \times 10^{-5}$ for **2**; $J = -1.15$ cm^{-1}, $g = 2.17$, $\theta = -0.02$ K, and $R = 1.4 \times 10^{-5}$ for **6**; and $J = -0.92$ cm^{-1}, $g = 2.14$, $\theta = -0.01$ K, and $R = 1.1 \times 10^{-5}$ for **6**. The Weiss parameter θ was introduced to account for the interdimer magnetic interactions. This simple model reproduces very well the magnetic data of all three compounds.

The values of the magnetic coupling through the double dca bridge in **2**, **6**, and **10** are small, antiferromagnetic, and very close to each other. Weak antiferromagnetic interactions between high-spin iron(II) ions through single and double $\mu_{1,5}$-dca bridges were observed in the few reports concerning this type of compound.[29c,44−46] It deserves to be outlined that a value of $J = -0.8$ cm^{-1} was determined for the high-spin iron(II) dinuclear complex of formula [(dca)(tpm)Fe($\mu_{1,5}$-dca)$_2$Fe(tpm)(dca)] [tpm = tris(pyrazolyl)methane][46] in good agreement with the J values for **2**, **6**, and **10**, and a weaker antiferromagnetic interaction ($J = -0.3$ cm^{-1}) was reported for the high-spin iron(II) complex [Fe(dca)$_2$(bipy)(H$_2$O)] where the iron atoms are connected through single $\mu_{1,5}$-dca bridges.[45]

The magnetic properties of compounds **3**, **7**, and **11** in the form of $\chi_M T$ versus T plots [χ_M is the magnetic susceptibility per one Co(II) ion] are shown in Figure 9. At room temperature, the values of $\chi_M T$ are 2.85 (**3**), 2.63 (**7**), and 2.80 $cm^3\ mol^{-1}$ K (**11**) [μ_{eff} per Co(II) = 4.77 (**3**), 4.59 (**7**), and 4.73 $N_A\beta$ (10), N_A being the Avogadro constant and β being the Bohr magneton] in agreement with one spin $S = 3/2$ with unquenched angular momentum [$\mu_{eff(spin\ only\ for\ g=2.0)} = 3.87\ N_A\beta$]. When the temperature is lowered, $\chi_M T$ slowly decreases and reaches 1.82 (**3**), 1.55 (**7**), and 1.57 $cm^3\ mol^{-1}$ K (**11**) at 1.9 K. The decrease may be the result of an antiferromagnetic coupling between the cobalt(II) ions or of the depopulation of the higher-energy Kramers doublets of the cobalt(II) centers.[47] Although the six-coordinated Co(II) ions in **3**, **7**, and **11** can be described as axially distorted in a symmetry close to C_{2v}, we have assumed that the rhombicity is close to zero to avoid an overparametrization in the analysis of the magnetic data of this family of complexes. Consequently, a symmetry close to C_{4v} results. Under an axial distortion, the triplet-orbital $^4T_{1g}$ ground state splits into singlet $^4A_2$ and doublet ^4E levels with a Δ energy gap. These considerations together with the satisfactory results obtained for the above systems through a dimer model moved us to analyze the magnetic data of **3**, **7**, and **11** through the Hamiltonian (eq 1)

$$\hat{H} = -J\hat{S}_1\hat{S}_2 - \sum_{i=1}^{2} \alpha_i\lambda_i\hat{L}_i\hat{S}_i + \sum_{i=1}^{2} \Delta_i[\hat{L}_{zi}^2 - 2/3] + \beta H \sum_{i=1}^{2} (-\alpha_i\hat{L}_i + g_e\hat{S}_i) \quad (1)$$

where the first term corresponds to the isotropic spin interaction, the second one is the spin−orbit coupling for each center, the third one accounts for the axial distortion of the T_1 orbital triplet in the A_2 singlet and E doublet terms ($\Delta > 0$ means that A_2 is the ground term), and the last one

(40) Manson, J. L.; Incarvito, C. D.; Arif, A. M.; Rheingold, A. L.; Miller, J. S. *Mol. Cryst. Liq. Cryst.* **1999**, *334*, 605.
(41) Wang, Z. M.; Sun, B. W.; Luo, J.; Gao, S.; Liao, C. S.; Yan, C. H.; Li, Y. *Inorg. Chim. Acta* **2002**, *332*, 127.
(42) Konar, S.; Dalai, S.; Ribas, J.; Drew, M. G.; Zangrando, E.; Chaudhuri, N. R. *Inorg. Chim. Acta* **2004**, *357*, 4208.
(43) Zu, L. N.; Ou-Yang, Y.; Liu, Z.-Q.; Liao, D.-Z.; Jiang, Z.-H.; Yan, S.-P.; Cheng, P. Z. *Anorg. Allg. Chem.* **2005**, *631*, 1693.
(44) Marshall, S. R.; Incarvito, C. D.; Manson, J. L.; Rheingold, A. L.; Miller, J. S. *Inorg. Chem.* **2000**, *39*, 1969.
(45) Martín, S.; Gotzone Barandika, M.; Ezpeleta, J. M.; Cortés, R.; Ruiz de Larramendi, J. I.; Lezama, L.; Rojo, T. *J. Chem. Soc., Dalton Trans.* **2002**, 4275.
(46) Batten, S. R.; Bjernemose, J.; Jensen, P.; Leita, B. A.; Murray, K. S.; Moubaraki, B.; Smith, J. P:; Toflund, H. *Dalton Trans.* **2004**, 3370.
(47) Banci, L.; Bencini, A.; Gatteschi, D.; Zanchini, C. *Struct. Bonding (Berlin)* **1982**, 52, 37.

Table 5. Selected Magnetostructural Data for Single and Double End-to-End Dca-Bridged Compounds[a]

formula		dca coordination mode	M···M	*J*	ref
$Mn(dca)_2(phen)$	2D	single and double	8, 0576(s) 7, 2049(d)	−1, 3	1
$Mn(dca)_2(bipy)$	1D	double	7, 512	−0, 17 −0, 4	9e−40, 12
$[Mn(dca)_2bpym]$	1D	double		−0, 18	30
$[Mn(dca)_2bpym]\cdot H_2O$	1D	single	8, 983	−0, 15	44
$Mn(dca)_2(dpp)$	2D	single	6, 909	−0, 26	22a
$Mn(dca)_2(H_2biim)$	1D	single	7, 549(3)	−0, 74	8
$[Mn(MAC)(dca)\}](PF_6)$	1D	single	7, 701	−0, 49	18b
$[Mn(dca)(NO_3)(terpy)]_n$	1D	single	8, 147	−0, 12	18c
[Mn(dca)(Oac)(terpy)	1D	single	8, 396	−0, 09	11
$[Mn(dca)(H_2O)(terpy)]_n[dca]_n$	1D	single	7, 574	−0, 20	18c
$Mn(dca)_2(py)_2$	1D	double	7, 5212	−0, 12	9e−13
$Mn(dca)_2(pic)_2$	1D	double	7, 457	−0, 33	8
$Mn(dca)_2(4CN\text{-}py)_2$	2D	single	8, 286	−0, 154	14a
$Mn(dca)_2(pdz)_2$	1D	double	7, 432	−0, 75	11
$Mn(dca)_2(NH_2\text{-}pyz)(H_2O)\cdot(NH_2\text{-}pyz)$	ladder	single and double	7, 45(d) 7, 51(s)		14b
$Mn(dca)_2(pyr)_2$	1D	double	7, 03	−0, 8	9d
$Mn(dca)_2(4\text{-}bzpy)_2$	1D	double	7, 584	−0, 3	12
$[Mn(dca)_2(4,4'\text{-}bipy)]\cdot 3/2H_2O$	tubes	single	7, 949 8, 326	−0, 24	9e−40
$Mn(dca)_2(4,4'\text{-}bipy)(H_2O)\cdot{}^1/_2MeOH$	tubes	single	8, 191 8, 349 8, 324 7, 771	−0, 104	29c
$[Cu(en)_2][Mn(dca)_4]$	1D	double	7, 625	−0, 12	41
$Mn(dca)_2(im)_2$	1D	double	7, 529	−0, 21	42
$[Mn(azpy)_2(dca)(H_2O)_2](ClO_4)(azpy)(H_2O)_2$	1D	single	8, 425	−0, 16	43

[a] Abbreviations: phen = phenanthroline, bipy = 2,2′-bipyridine, bpym = 2,2′-bipyrimidine, dpp = 2,3-bis(2-pyridyl)pyrazine, H_2biim = 2,2′-biimidazole, MAC =1,3-dimethyl-3,6,9,12,18-pentaazabicyclo[12.3.1]octadeca-1(18),2,12,14,16-pentaene, terpy = 2,2′:6′,2″-terpyridine, py = pyridine, pic = 4-picoline, 4CN-py = 4-cyanopyridine, pdz = pyridazine, NH_2-pyz = 2-aminopyrazine, pyr = 2-pyrrolidone, 4-bzpy = 4-benzoylpyridine, 4,4′-bipy = 4,4′-bipyridine, im = imidazole, azpy = 4,4′-azopyridine, en = ethylenediamine.

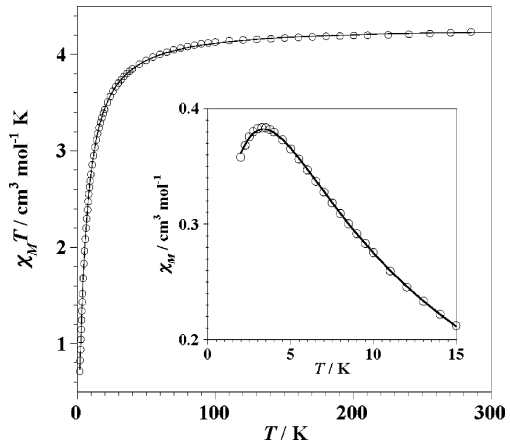

Figure 6. $\chi_M T$ vs T plot for complex **1**: (○) experimental data and (−) best-fit curve (see text). The inset shows the χ_M vs T plot in the vicinity of the maximum.

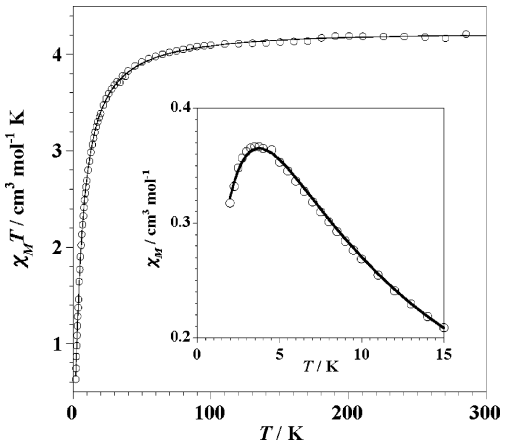

Figure 7. $\chi_M T$ vs T plot for complex **5**: (○) experimental data and (−) best-fit curve (see text). The inset shows the χ_M vs T plot in the vicinity of the maximum.

is the Zeeman effect. α is the orbital reduction factor defined as $\alpha = A\kappa$, where κ is the reduction factor resulting from the covalent bond and A is a factor of the isomorphism between the orbital angular moment operator in T_1 and P bases, $\mathbf{L}(T_1) = -A\mathbf{L}(P)$.[48] This factor takes into account the mixture between the $^4T_1$ levels from the ^4F and ^4P terms (*A* varies between 3/2 and 1 for weak and strong ligand-field limits, respectively). No analytical expression for the magnetic susceptibility as a function of α, Δ, λ, and *J* can be derived, and the values of these parameters were determined through numerical matrix diagonalization. The best-fit parameters of the experimental data in the whole temperature range are $\alpha = 1.32$, $\Delta = -1000$ cm^{-1}, $\lambda = -130$ cm^{-1}, $J = -0.33$ cm^{-1}, and $\theta = -0.017$ K (**3**); $\alpha = 1.11$, $\Delta = -630$ cm^{-1}, $\lambda = -165$ cm^{-1}, $J = -0.17$ cm^{-1}, and $\theta = -0.009$ K (**7**); and $\alpha = 1.07$, $\Delta = -330$ cm^{-1}, $\lambda = -170$ cm^{-1}, $J = -0.03$ cm^{-1}, and $\theta = -0.005$ K (**11**). θ is an additional Weiss term which accounts for the interdimer magnetic coupling. The theoretical curves reproduce very well the magnetic data in the whole temperature range. The values of α, λ, and Δ are within the range of those reported for

(48) Herrera, J. M.; Bleuzen, A.; Dromzée, Y.; Julve, M.; Lloret, F.; Verdaguer, M. *Inorg. Chem.* **2003**, *42*, 7052.

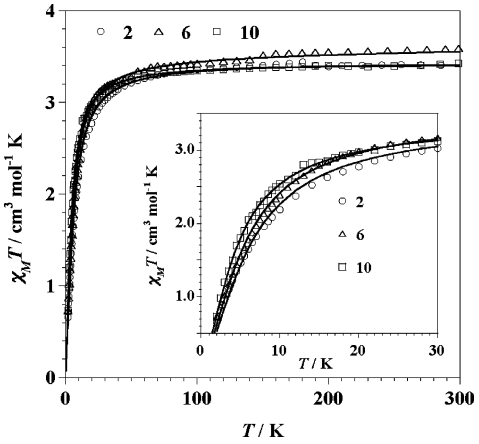

Figure 8. $\chi_M T$ vs T plots for complexes **2**, **6**, and **8**. The solid lines are the best-fit curves (see text), and the insets show the low-temperature region in detail.

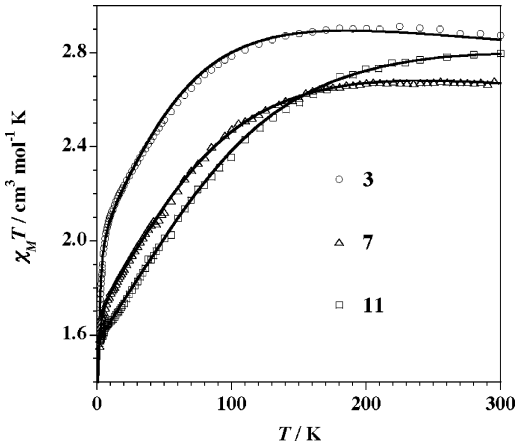

Figure 9. $\chi_M T$ vs T plots for complexes **3**, **7,** and **11**. The solid lines are the best-fit curves (see text).

high-spin octahedral Co(II) complexes. The values of λ are slightly smaller than that of the free ion ($\lambda_o = -180$ cm^{-1}) because of covalency effects. Finally, the small values of the energy gap, Δ, indicate a weak distortion, in agreement with the values of the magnetic moment at room temperature.

The values of the magnetic coupling through the double end-to-end dca bridges in **3**, **7**, and **11** are very weak. A literature survey shows that, in general, the magnetic data of mixed-ligand Co(II)/dca/L compounds have been interpreted successfully as a combination of spin−orbit coupling and low-symmetry ligand-field effects or well using a Curie-Weis law with a θ term accounting for these parameters plus the possible weak magnetic interactions.[21,29c,49] This is why a comparison of the J values that we obtained for **3**, **7**, and **11** with other values from the literature are practically precluded. Anyway, it deserves to be pointed out that our results are in agreement with the weak antiferromagnetic interaction of ca. -1.0 cm^{-1} which was reported for the chain compound $[Co(dca)_4(bpym)]_n \cdot nH_2O$, where the high-spin

(49) (a) Jensen, J.; Batten, S. R.; Moubaraki, B.; Murray, K. S. *J. Solid State Chem.* **2001**, *159*, 352. (b) Kutasi, A. M.; Batten S. R.; Harris, A. R.; Moubaraki, B.; Murray, K. S. *CrystEngComm* **2002**, *4*, 202. (c) Gao, E. Q.; Bai, S. Q.; Wang, Z. M.; Yan, C. H. *Dalton Trans.* **2003**, 1759. (d) Sun, H. L.; Gao, S.; Ma, B. Q.; Batten, S. R. *CrystEngComm* **2004**, *6*, 579.

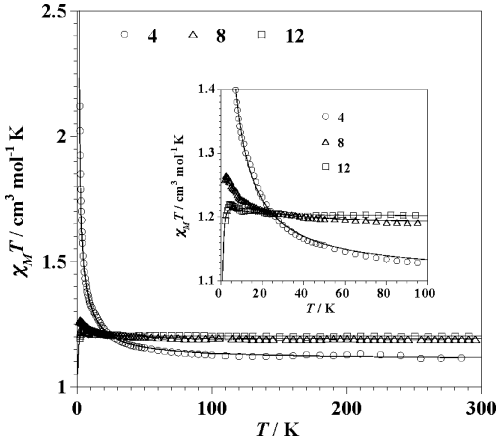

Figure 10. $\chi_M T$ vs T plots for complexes **4**, **8**, and **12**. The solid lines are the best-fit curves (see text), and the inset show the low-temperature region in detail.

Co(II) ions are linked through single end-to-end dca bridges.[44] This confirms the poor ability of the dca bridge to mediate magnetic interactions between the spin carriers when adopting the μ-1,5 bridging mode.

The magnetic properties of compounds **4**, **8**, and **12** in the form of $\chi_M T$ versus T plots [χ_M is the magnetic susceptibility per one Ni(II) ion] are shown in Figure 10. At room temperature, the values of $\chi_M T$ are 1.15 (**4**) and 1.20 cm^3 mol^{-1} K (**8** and **12**). They are all as expected for a magnetically isolated spin triplet ($\chi_M T = 1.10$ cm^3 mol^{-1} K with $g = 2.10$). These values remain practically constant when cooling until 10 (**8** and **12**) and 80 K (**4**), and they increase smoothly (**8** and **12**) and sharply (**4**) at lower temperatures. A maximum of $\chi_M T$ is observed for **8** and **12** at 3.0 and 4.0 K, respectively, whereas the $\chi_M T$ values continuously increase for **4** to reach a value of 1.40 cm^3 mol^{-1} K at 1.9 K. These features are indicative of the occurrence of weak ferromagnetic interactions in all three compounds. Most likely, the small decrease of $\chi_M T$ at very low temperatures for **8** and **12** may be due to zero-field splittings effects. Keeping these features in mind and following the same methodology that we used for the previous compounds, we have analyzed the magnetic data of **4**, **8**, and **12** through the analytical expression for a nickel(II) dimer which was derived by Ginsberg et al.[50] by using the spin Hamiltonian (eq 2)

$$\hat{H} = -JS_A S_B - D(S_{zA}^2 + S_{zB}^2) - z'J'S_z\langle S_z\rangle \qquad (2)$$

where the last term takes into account the interdimer interactions in the context of the molecular field approximation. J, D, S_z, z', and J' are the intradimer magnetic interaction, the zero field splitting of the nickel(II) ion, the operator for the z component of the total dimer spin, the dimer lattice coordination number, and the effective interdimer magnetic coupling, respectively. The least-squares fits led to the following set of parameters: $J = +1.02$ cm^{-1}, $g = 2.11$, $D = 4.6$ cm^{-1}, and $z'J' = +0.083$ cm^{-1} for **4**; $J = +0.20$ cm^{-1}, $g = 2.18$, $D = 2.58$ cm^{-1}, and $z'J' = +0.005$

(50) Ginsberg, A. P.; Martin, R. L.; Brookes, R. W.; Sherwood, R. C. *Inorg. Chem.* **1972**, *11*, 2884.

cm^{-1} for **8**; and $J = +0.05\ cm^{-1}$, $g = 2.19$, $D = 1.62\ cm^{-1}$, and $z'J' = +0.002\ cm^{-1}$ for **12**. It was assumed that $g_x = g_y = g_z = g$. The calculated curves match the magnetic data in the whole temperature range very well.

Interestingly, the magnetic interactions in the dca-bridged nickel(II) derivatives **4**, **8**, and **12** are again weak, but they are ferromagnetic in nature. Both the intra- and interdimer magnetic couplings are positive. This result agrees with those obtained in a few examples of mixed-ligand Ni(II)/dca/L systems where the dca exhibits the end-to-end bridging mode (J values varying between ca. $+1.0$ and $+0.7\ cm^{-1}$).[45,51] According to MO calculations performed on the dca ligand and on dinuclear models with a single end-to-end dca bridge,[12] from the two exchange pathways which are possible in this kind of complex, namely $e_g-\sigma-e_g$ and $t_{2g}-\pi-t_{2g}$, only the first one would be effective because of the e_g nature of the magnetic orbitals of the six-coordinated nickel(II) ion. It is found that this pathway leads to a net overlap close to zero for values of the M−N−C(dca) angle close to 160−170°. Consequently, the weak ferromagnetic coupling observed for this type of dca-bridged nickel(II) complexes could be the result of a case of accidental orthogonality. Of course, more examples of this type of complex and a deeper theoretical study (DFT-type calculations, for instance) are needed in order to substantiate this hypothesis.

Conclusions

We would like to conclude this contribution by focusing on the design of novel polymeric architectures obtained using the dca anion and α-diimine molecules as ligands toward divalent first-row transition metal ions. Polymeric complexes of formula $M(dca)L_nX$ ($n = 1$ or 2, L = α-diimine ligand, and X = a monovalent anion such as ClO_4^-, Cl^-, NO_3^-, or CH_3COO^-) are 1D compounds built by a single dca bridge in the $\mu_{1,5}$ end-to-end coordination mode.[10,17,20,21,52] Also the polymers $M(dca)_2L{\cdot}nH_2O$ ($n = 0$ or 1) are mostly chains exhibiting two types of 1D structures: (i) chains in which one dca acts as a single $\mu_{1,5}$ bridge and the other is terminal[8,19,20,44,53] and (ii) zigzag chains in which each metal ion is coordinated by four $\mu_{1,5}$ dca groups which form two double bridges.[12,30] Complexes of higher dimensionality are scarce. Only a 3D network has been obtained containing the radical 2-(2-thiazole)-4,4,5,5-tetramethyl-4,5-dihydro-1*H*-imidazolyl-1-oxy-3-oxide as a ligand.[28] There are few examples of compounds showing a 2D architecture. Square-grids (4,4) are formed when the chelating ligand is 2,3-bis-(2-pyridyl)pyrazine,[22a] 2,2′-biimidazoline,[16] and 1-(2-aminoethyl)piperidine.[25b] Each metal atom, in these compounds, is connected to other four metal centers by means of single dca bridges in the $\mu_{1,5}$[16,22a] or $\mu_{1,3}$[25b] coordination modes. In contrast, in the compounds of general formula $[M(dca)_2(phen)]$, M = Mn,[23] Cu,[24] Cd,[26] or Zn,[25] the structure is made up of (6,3) grids and both double and single dca bridges occur. It is noteworthy that the 1D and 2D structures of these last compounds can have the same general formula. This feature suggests that the nature of the α-diimine ligand can affect the dimensionality of the resulting framework. Keeping this in mind, we have expanded the investigation on 2D systems involving phen, dca, and Mn(II), Fe(II), Co(II), and Ni(II) cations. To clarify how the introduction of methyl substituents in different positions can induce modifications on the architecture of the resulting compounds, we also used 4,7-dmphen and 2,9-dmphen as ligands. Our results indicate that the phen and 4,7-dmphen ligands produce compounds that are isostructural to the previously reported phen complexes. On the contrary, the introduction of the methyl substituents ortho to the nitrogen atoms results in an unprecedented 2D architecture. We can conclude that the ancillary ligand leads to the formation of different networks depending on the position of the methyl substituent position.

The magnetic studies indicate that complexes of Mn, Fe, and Co exhibit weak antiferromagnetic interactions, while the dca-bridged Ni(II) derivatives are weakly ferromagnetic. Keeping in mind that a ferromagnetic coupling was observed for the analogue compound $[Cu(dca)_2(phen)]$, one can conclude that the magnetic behavior among divalent first-row transition metal ions changes from antiferromagnetic to ferromagnetic in the Mn to Cu series. In a near future, theoretical studies will be performed to get a clear orbital picture of this interesting feature.

Acknowledgment. This research was supported by the Italian Ministero dell'Istruzione, dell'Università e della Ricerca, the Ministerio Español de Ciencia y Tecnología (Project CTQ2004-03633) and the Agencia Valenciana de Ciencia y Tecnología (Grupos 03/197).

Supporting Information Available: X-ray crystallographic files in CIF format, tables of the bond lengths and angles related to the dca ligands (Tables S1 and S2), a complete list of intralayer M···M distances (Tables S3 and S4), perspective view of the 2D herringbone grid of frameworks **5**−**8**, and $\chi_M T$ versus T plot for complex **9** (Figure S1 and S2, respectively). This material is available free of charge via the Internet at http://pubs.acs.org.

IC060044U

(51) Ghoshal, D.; Bialas, H.; Escuer, A.; Font-Bardía, M.; Maji, T. K.; Ribas, J.; Solans, X.; Vivente, R.; Zangrando, E.; Chaudhuri, N. R. *Eur. J. Inorg. Chem.* **2003**, 3929. (b) Colacio, E.; Maimoun, K. R.; Sillanpää, R.; Suárez-Varela, J. *Inorg. Chim. Acta* **2004**, *357*, 1465.

(52) (a) Wu, A. Q.; Cai, L. Z.; Chen, W. T.; Guo, G. C.; Huang, J. S. *Acta Crystallogr., Sect. C* **2003**, *59*, M491. (b) Wu, A. Q.; Zheng, F. K.; Cai, L. Z.; Guo, G. C.; Mao, J. G.; Huang, J. S. *Acta Crystallogr., Sect. E.* **2003**, *59*, M257.

(53) Kou, H. Z.; He, Y. *Chem. Lett.* **2003**, *32*, 902.